





## Binder ratio in the two-dimensional $q$ -state clock model

Luong Minh Tuan <sup>1,2</sup> Ta Thanh Long <sup>1</sup> Duong Xuan Nui <sup>1,3</sup> Pham Tuan Minh,<sup>4</sup>  
 Nguyen Duc Trung Kien,<sup>1</sup> and Dao Xuan Viet <sup>1</sup>

<sup>1</sup>*Advanced Institute for Science and Technology, Hanoi University of Science and Technology, Hanoi 10000, Vietnam*

<sup>2</sup>*Faculty of Mechanical Engineering, National University of Civil Engineering, Hanoi 10000, Vietnam*

<sup>3</sup>*Faculty of Electromechanical and Civil Engineering, Vietnam National University of Forestry, Hanoi 10000, Vietnam*

<sup>4</sup>*Institute of Physics, Vietnam Academy of Science and Technology, Hanoi 10000, Vietnam*



(Received 1 May 2021; revised 24 July 2022; accepted 12 September 2022; published 30 September 2022)

We study phase transition properties of the two-dimensional  $q$ -state clock model by an extensive Monte Carlo simulation. By analyzing the Binder ratio and its temperature derivative, we confirm that the two-dimensional  $q$ -state clock model exhibits two distinct Kosterlitz-Thouless phase transitions for  $q = 5, 6$  but it has one second-order phase transition for  $q = 4$ . The critical temperatures are estimated quite accurately from the crossing behavior of the Binder ratio (for  $q < 5$ ) and from negative divergent dips of the derivative of the Binder ratio (for  $q \geq 5$ ) around these critical points. We also calculate the correlation length, the helicity modulus, and the derivative of the helicity modulus, and analyze their behaviors in different phases in detail.

DOI: [10.1103/PhysRevE.106.034138](https://doi.org/10.1103/PhysRevE.106.034138)

### I. INTRODUCTION

The two-dimensional (2D)  $q$ -state clock model has been studied extensively in phase transition phenomena for years [1–9]. It is a generalization of the 2D Ising model for  $q = 2$ , but it approaches the 2D  $XY$  model in the limit  $q \rightarrow \infty$ . The 2D Ising model exhibits a second-order phase transition between the long-range ordered phase and the disordered phase. For the 2D  $XY$  model, in early days it was indicated that there is no sign of a phase transition [10]. But then it was proved to have the Kosterlitz-Thouless (KT) phase transition between the quasi-long-range ordered phase and the disordered phase [11]. The KT phase transition is one of the most important concepts in statistical physics. The KT phase transition is observed in many 2D systems, such as a planar array of coupled Josephson junctions in a transverse magnetic field [12], a liquid crystal [13], and a 2D Coulomb crystal [14]. Interestingly, this type of phase transition also appears in the 2D  $q$ -state clock model, depending on the number of single spin states  $q$ .

It was theoretically predicted [1] and later confirmed by several numerical works [2–4] that the 2D  $q$ -state clock model has only one second-order phase transition at  $T_c$  for  $q < 5$  and two distinct KT phase transitions at finite critical temperatures  $T_1$  and  $T_2$  ( $T_2 > T_1$ ) for  $q \geq 5$ . The intermediate phase between these critical temperatures is a quasi-long-range ordered phase like that of the 2D  $XY$  model. The phase above  $T_2$  is a disordered phase, and the phase below  $T_1$  is a long-range ordered phase [2].

Recently, Monte Carlo simulation studies of phase transitions in the 2D  $q$ -state clock model have mainly tried to clarify  $q_c$ , the critical value of the boundary between the KT transition type (for  $q \geq q_c$ ) and the non-KT transition type (for  $q < q_c$ ). From the behavior of the helicity modulus and the fourth-order helicity modulus, Lapilli *et al.* [15] claimed

that the KT transitions occur only for  $q \geq 8$ . Based on the helicity modulus and its temperature derivative, Baek *et al.* [6] concluded that the transitions are KT type for  $q \geq 6$ . However, more recent studies [8,9,16] are in favor of the previous scenario where  $q_c = 5$ . Kumano *et al.* [8] and Chatelain *et al.* [16] demonstrated that the 2D five-state clock model exhibits two KT phase transitions via the behavior of the discrete helicity modulus. Surungan *et al.* [9] approached in a different way: they calculated correlation lengths for both the 2D  $q$ -state clock model and the Villain model. By comparing the behavior of correlation lengths of these two models, they also argued about having two KT transitions for  $q = 5$ . The phase transition type of the model in case of  $q = 5$  is controversial because its different physical quantities lead to different results of  $q_c$ . For  $q = 5$ , while the helicity modulus shows the behavior of non-KT phase transitions [6], the discrete helicity modulus [8] and the correlation length [9] show the behavior of KT phase transitions, but it seems to be unclear because of the narrow intermediate phase.

In order to clarify further the type of phase transitions in the 2D  $q$ -state clock model, we perform an extensive Monte Carlo simulation but focus on  $q = 4, 5$ , and 6. We calculate several independent physical quantities including the Binder ratio, the derivative of the Binder ratio, the correlation length ratio, the helicity modulus, and the derivative of the helicity modulus.

### II. MODEL AND METHODS

The  $q$ -state clock model in a square lattice is defined by the Hamiltonian

$$H = -J \sum_{\langle ij \rangle} \cos(\theta_i - \theta_j), \quad (1)$$

where  $\theta_i$  and  $\theta_j$  are the angles of spins with respect to the  $x$  axis at sites  $i$  and  $j$ , respectively.  $\theta_i = 2\pi\sigma_i/q$  and  $\theta_j = 2\pi\sigma_j/q$  with  $\sigma_i, \sigma_j \in 0, 1, \dots, q-1$ . The coupling  $J$  is the interaction strength, considered as the basic energy scale and set to 1 throughout this work. Each spin interacts with all of its nearest neighbor spins.

For  $q = 2$ , the model becomes the 2D Ising model (spin has two possible values); for  $q = \infty$ , the model becomes the 2D  $XY$  model (infinity of possible values). In this work, we focus on the cases  $q = 4$ ,  $q = 5$  and  $q = 6$  only. The simulation is taken on a square lattice of size  $L$  with the total site number  $N = L^2$ . The value  $L$  is chosen from 16 to 256, and we include additional values  $L = 512, 1024$  for the  $q = 5$  case. Here we use periodic boundary conditions for this lattice in both directions.

We carry out an equilibrium Monte Carlo (MC) simulation by using a combination of the Metropolis algorithm (single spin flip) and the Wolff algorithm (cluster spin flip). Our unit MC step includes one Metropolis sweep and one Wolff sweep. The Monte Carlo simulation parameters for each case are shown in Table I, where  $L$  is the system size,  $N_r$  is the number of independent runs,  $N_{MC}$  is the total number of MC steps, and  $N_T$  is the number of temperature points. The first half of total MC simulation steps is discarded and the second half is used to measure physical quantities. An equality of specific heat capacities computed by the energy fluctuation and via the temperature difference of the energy is checked to identify the thermal equilibrium condition. After reaching the equilibrium in the system, we measure several physical quantities, including the helicity modulus, the temperature derivative of the helicity modulus, the correlation length ratio, the Binder ratio, and the temperature derivative of the Binder ratio.

The helicity modulus and its temperature derivative are defined by [6]

$$\Upsilon = \langle e \rangle - \frac{L^2}{T} \langle s^2 \rangle, \quad (2)$$

$$\frac{d\Upsilon}{dT} = \frac{1}{T^2} \left[ \langle eH \rangle - \langle e \rangle \langle H \rangle + L^2 \langle s^2 \rangle - \frac{L^2}{T} (\langle s^2 H \rangle - \langle s^2 \rangle \langle H \rangle) \right], \quad (3)$$

where  $e = 1/L^2 \sum_{(ij)_x} \cos(\theta_i - \theta_j)$ ,  $s = 1/L^2 \sum_{(ij)_x} \sin(\theta_i - \theta_j)$ , the sum is taken over all links in one direction, and  $\langle \dots \rangle$  stands for the thermal average.

The second-moment correlation length is defined as [17–19]

$$\xi = \frac{1}{2 \sin(k_m/2)} \sqrt{\frac{\langle m(\vec{0})^2 \rangle}{\langle m(\vec{k}_m)^2 \rangle} - 1}, \quad (4)$$

where  $k_m = 2\pi/L$  and  $\vec{k}_m = (k_m, 0)$ . The  $k$ -dependent magnetization is expressed as

$$m(\vec{k})^2 = \sum_{\mu=x,y} \left| \frac{1}{N} \sum_{i=1}^N S_{i\mu} \exp(i\vec{k} \cdot \vec{r}_i) \right|^2. \quad (5)$$

The projections of the spin at site  $i$  on the  $x$  axis and the  $y$  axis are  $S_{ix} = \cos \theta_i$  and  $S_{iy} = \sin \theta_i$ , respectively. For a second-order phase transition,  $\xi/L$  of different sizes  $L$  approximately cross at the critical temperature [17,20]. For a KT

TABLE I. Various parameters of our Monte Carlo simulations.  $L$  is the system size,  $N_r$  is the number of independent runs,  $N_{MC}$  is the total number of MC steps, and  $N_T$  is the total number of temperature points.

	$L$	$N_r$	$N_{MC}$	$N_T$
$q = 4$	16	5	$2.10^6$	39
	32	5	$2.10^6$	39
	64	5	$2.10^6$	39
	128	5	$2.10^6$	39
	256	5	$3.10^6$	25
$q = 5$	16	5	$2.10^6$	75
	32	5	$2.10^6$	75
	64	5	$2.10^6$	75
	128	5	$2.10^6$	75
	256	5	$3.10^6$	60
	512	5	$4.10^6$	26
	1024	5	$4.10^6$	23
$q = 6$	16	5	$2.10^6$	77
	32	5	$2.10^6$	77
	64	5	$2.10^6$	77
	128	5	$2.10^6$	77
	256	5	$3.10^6$	74

phase transition,  $\xi/L$  of different sizes  $L$  merge at the critical point [17,21,22]. The Binder ratio is another suitable quantity to verify a phase transition [17,21,23,24]:

$$g = 2 - \frac{\langle m^4 \rangle}{\langle m^2 \rangle^2}, \quad (6)$$

where  $m^2 = m(\vec{0})^2$  and  $m^4 = m(\vec{0})^4$ . For the 2D Ising model, the Binder ratio shows a crossing behavior at the second-order phase transition, which is quite similar to  $\xi/L$ . For the 2D  $XY$  model, the Binder ratio shows a merging behavior at the KT phase transition as well as  $\xi/L$  [17]. Based on the relation  $\partial g(L)/\partial g(L)|_{T=T_c} = (L/L)^{1/\nu}$  [25,26], one can obtain the critical exponent  $\nu$ , where  $1/\nu$  is nonzero for a second-order phase transition and zero for a KT phase transition. It indicates that estimating critical temperatures is easy in second-order phase transitions but difficult in KT phase transitions. Similarly to  $d\Upsilon/dT$ , we also use  $dg/dT$  to estimate critical points [15]:

$$\frac{dg}{dT} = \frac{1}{T^2} \left( -\frac{\langle m^4 H \rangle}{\langle m^2 \rangle^2} + \frac{2\langle m^4 \rangle \langle m^2 H \rangle}{\langle m^2 \rangle^3} - \frac{\langle m^4 \rangle \langle H \rangle}{\langle m^2 \rangle^2} \right). \quad (7)$$

The temperature derivative of the Binder ratio diverges at the critical temperature as  $L \rightarrow \infty$ .

### III. SIMULATED RESULTS

In this section, we present our numerical results of several physical quantities including the Binder ratio and its temperature derivative, the correlation length ratio, and the helicity modulus and its temperature derivative.

For convenience of notation, let  $T_c$  denote the critical temperature of the unique phase transition for  $q < 5$ . For  $q \geq 5$ , these exist two phase transitions. The lower critical temperature (between the long-range ordered phase and the

quasi-long-range ordered phase) is denoted as  $T_1$ , while the higher critical temperature (between the quasi-long-range ordered phase and the disordered phase) is denoted as  $T_2$ . These critical temperatures ( $T_c$ ,  $T_1$ , and  $T_2$ ) will be estimated by the Binder ratio and its temperature derivative.

Figure 1 shows the Binder ratio  $g$  versus temperature for  $q = 4, 5, 6$ . For  $q = 4$  [see Fig. 1(a)],  $g$  curves of different system sizes  $L$  cross nearly at the critical point, this is the behavior of a second-order phase transition. In order to extrapolate the critical temperature  $T_c$  in the thermodynamic limit  $L \rightarrow \infty$ , we estimate the crossing temperature  $T_c(L)$  between  $g(L)$  and  $g(L/2)$ . Then, the critical temperature  $T_c = 1.135$  is obtained by fitting  $T_c(L)$  in the following form:

$$T_c(L) = T_c + bL^{-1/\nu}. \quad (8)$$

For  $q = 5, 6$  [see Figs. 1(b) and 1(c)],  $g(T)$  curves of different  $L$  increase upward to 1 in the low-temperature region, and decrease downward to 0 in the high-temperature region. These are behaviors of the low-temperature ordered phase and the high-temperature disordered phase, respectively. Moreover, in the intermediate-temperature region between two phase transitions at  $T_1$  and  $T_2$ ,  $g(L)$  curves tend to merge to finite values less than 1 for large system sizes [ $L = 256, 512, 1024$  for  $q = 5$  in Fig. 1(b) and  $L = 64, 128, 256$  for  $q = 6$  in Fig. 1(c)]. This behavior of the Binder ratio resembles that of other models, such as the 2D TIAFF model with a KT phase between a ferromagnetic phase and a paramagnetic phase [27], and the 2D dimer model with a KT phase between a long-range ordered phase and a disordered phase [28]. In order to see more clearly the merging characteristic of  $g$  for  $q = 5$ , we plot the  $g(L)$  versus  $L$  at several temperatures ranging from 0.88 to 0.965 in the lower inset of Fig. 1(b). With increasing  $L$ ,  $g(L)$  increases monotonically up to 1 (characteristic of an ordered phase) for low temperatures  $T = 0.88, 0.89$ , decreases monotonically down to 0 (characteristic of a disordered phase) for high temperatures  $T = 0.955, 0.965$ , and is almost flat for intermediate temperatures  $T = 0.915, 0.920, 0.930, 0.945$ . It means that  $g(L)$  tends to be equal to  $g(L')$  for lattice size large enough at intermediate temperatures. Therefore,  $\partial g(L')/\partial g(L) = (L'/L)^{1/\nu} \approx 1$  for any temperature in range  $[0.915, 0.945]$ . This implies that  $\nu = \infty$  for any  $0.915 < T < 0.945$ , and consequently, the correlation length is exponentially divergent. This is a signal of the existence of a KT phase between  $T = 0.915$  and  $T = 0.945$ . It means that the phase transition at  $T_2$  is KT type between the disordered phase ( $g = 0$ ) and the KT phase, while the phase transition at  $T_1$  is also KT type between the KT phase and the ferromagnetic phase ( $g \rightarrow 1$ ).

It is difficult to estimate exactly the critical temperatures  $T_1$  and  $T_2$  from the Binder ratio in Fig. 1(b) for  $q = 5$  and Fig. 1(c) for  $q = 6$  due to ill-defined boundaries of the merging interval in the intermediate KT phase, i.e., the quasi-long-range ordered phase. Furthermore, Baek *et al.* discussed that the Binder ratio cannot be used to determine the critical temperature  $T_1$  between the long-range ordered phase and the quasi-long-range ordered phase in a generalized 2D  $q$ -state clock model [29]. They explained that this is due to the spin vectors of the long-range ordered phase and the quasi-long-range ordered phase which differ from each other only in the angular component. Then, Borisenko *et al.* proposed a

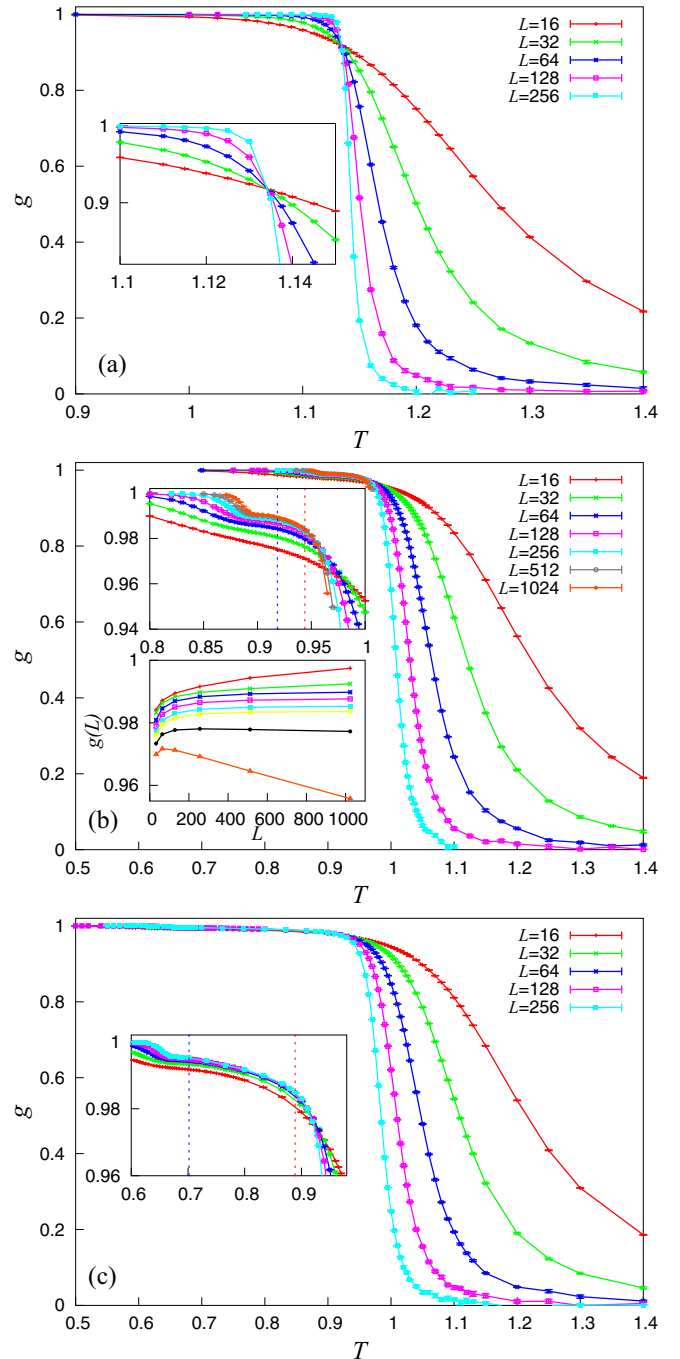


FIG. 1. Temperature dependence of the Binder ratio  $g$  for three cases:  $q = 4$  (a),  $q = 5$  (b), and  $q = 6$  (c). Enlarged plots show the crossing behavior of  $g(L)$  curves for  $q = 4$  [the inset of (a)] and represent the merging behavior of  $g(L)$  for  $q = 5, 6$  [the upper inset of (b) and the inset of (c)]. In order to show the merging characteristic of  $g(L)$  for  $q = 5$  clearly, we plot  $g(L)$  versus  $L$  in the lower inset (b) for several temperatures  $T = 0.88, 0.89, 0.915, 0.930, 0.940, 0.945, 0.955, 0.965$  from top to bottom.

modified Binder ratio based on the angular magnetization to estimate the critical temperature  $T_1$  of the five-state clock model [24]. However, we show here that the conventional Binder ratio is still capable of defining both the KT phase

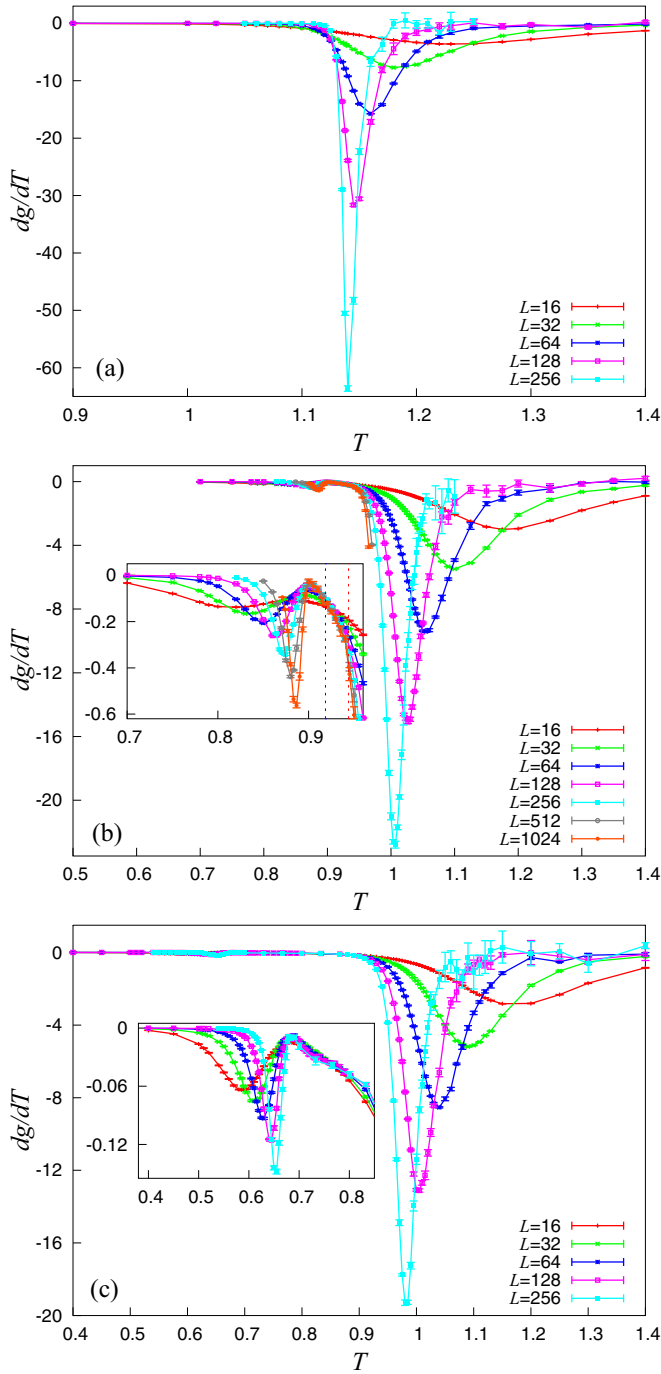


FIG. 2. The temperature derivative of the Binder ratio  $dg/dT$  versus temperature for three cases:  $q = 4$  (a),  $q = 5$  (b), and  $q = 6$  (c). Enlarged plots for  $q = 5$  and  $q = 6$  present a negative divergent dip around  $T_1$ .

transitions, not only between the disordered phase and the quasi-long-range ordered phase but also between the long-range ordered phase and the quasi-long-range ordered phase. Hence, we make an effort to estimate the critical temperatures precisely by using the temperature derivative of the Binder ratio  $dg/dT$ .

Figure 2 illustrates the temperature dependence of the derivative of the Binder ratio for  $q = 4, 5, 6$ . For  $q = 4$ ,

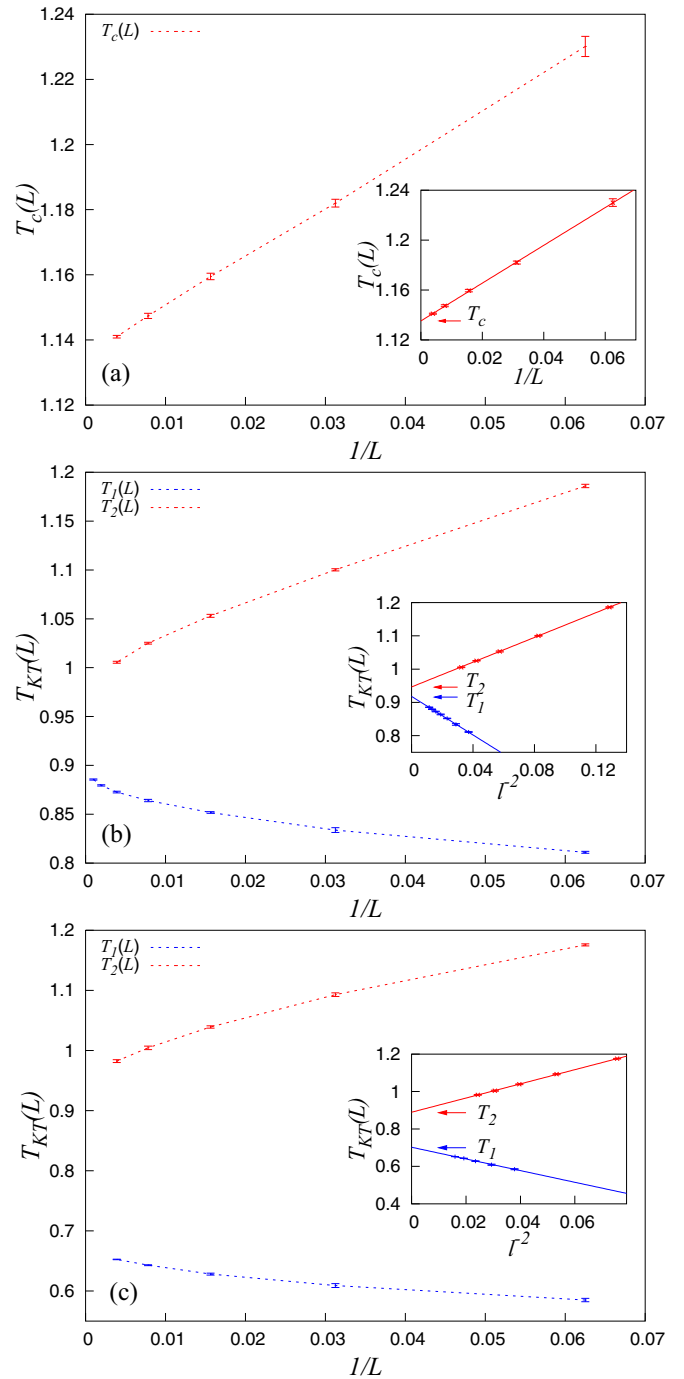
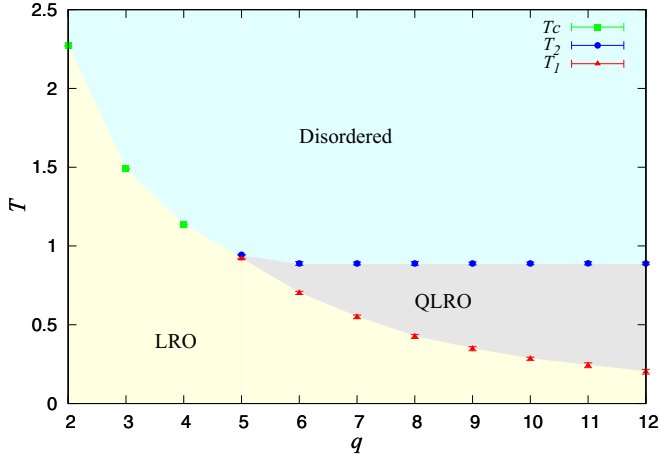


FIG. 3. The dip temperatures of  $dg/dT$  with their error bars as a function of  $1/L$  for  $q = 4$  (a),  $q = 5$  (b), and  $q = 6$  (c).  $T_c(L)$  of  $q = 4$  fits well by a linear function of  $1/L$  in the inset (a).  $T_{KT}(L)$  as a function of  $l^{-2}$  with  $l = \ln bL$  for  $q = 5$  in the inset (b) and for  $q = 6$  in the inset (c).

$dg/dT$  has a negative divergent dip at nearly  $T_c$  [see Fig. 2(a)]. The dip temperature  $T_c(L)$  gradually shifts toward  $T_c$  as  $L \rightarrow \infty$ .  $T_c(L)$  is a linear function of  $1/L$  in Fig. 3(a), hence it supports that the phase transition in the case  $q = 4$  is second order.

For  $q = 5$  and  $q = 6$ , there appear two negative divergent dipoles of  $dg/dT$ : a small one near  $T_1$  and a large one near  $T_2$  [see


 FIG. 4. The phase diagram of the 2D  $q$ -state clock model.

Figs. 2(b) and 2(c)]. As  $L \rightarrow \infty$ , both small dip temperature  $T_1(L)$  and large dip temperature  $T_2(L)$  gradually shift toward their respective critical temperatures  $T_1$  and  $T_2$ . The size dependences of  $T_1(L)$  and  $T_2(L)$  for  $q = 5, 6$  are non-linear in Figs. 3(b) and 3(c), meaning that the phase transitions at  $T_1$  and  $T_2$  are not second order.

In order to determine the critical points for  $q = 5$  and  $q = 6$ , we use the best fitting based on Eq. (9) [30]. The finite-size scaling, based on the form of correlation length near the critical temperature in a KT phase transition, is  $\xi(T) = A \exp(c/\sqrt{t})$ , with  $t = (T - T_{KT})/T_{KT}$ . We define  $T_{KT}(L)$  as the temperature at the dip bottom of  $dg/dT$ . Both  $g$  and  $\xi/L (= a)$  near the critical point are approximately independent of the system size  $L$ . Then, by using the finite-size scaling form of the Binder ratio,  $g = g(\xi/L)$ , we have the relation

$$T_{KT}(L) = T_{KT} + \frac{c^2 T_{KT}}{(\ln bL)^2}, \quad (9)$$

where  $b = a/A$ .

We plot  $T_{KT}(L)$  as a function of  $l^{-2}$  with  $l = \ln bL$  in the best parameter fit for  $q = 5$  in Fig. 3(b) and for  $q = 6$  in Fig. 3(c). For  $q = 6$ , best fits of  $T_{KT}(L)$  based on Eq. (9) give us  $T_1 = 0.702^{+0.010}_{-0.008}$  with  $b_1 = 10.67$  and  $T_2 = 0.889^{+0.011}_{-0.012}$  with  $b_2 = 2.38$ . The error bar is estimated by  $\chi^2$  analysis. These values are consistent with previous works [8,24]. For  $q = 5$ , we also estimate the critical temperatures by best fits of  $T_{KT}$  and get  $T_1 = 0.918^{+0.004}_{-0.004}$  with  $b_1 = 11.2$  and  $T_2 = 0.944^{+0.002}_{-0.003}$  with  $b_2 = 1.08$ . These critical temperature values,  $T_1$  and  $T_2$ , are consistent within errors with previous works [8,9]. Of course, we can estimate the critical temperature  $T_c$  for the  $q = 4$  case (or  $q \leq 4$  cases, in general) from the divergent dip temperature of the Binder ratio derivative as we do for  $q = 5, 6$  cases. We also obtain the same result of  $T_c$  as calculated from the crossing temperature of the Binder ratio. However, evaluating  $T_c$  for  $q \leq 4$  cases from the crossing temperature of  $g$  is simpler and more precise than from the dip temperature of  $dg/dT$ .

The phase diagram of the 2D  $q$ -state clock model obtained only by analyzing our Binder ratio is shown as in Fig. 4. For  $q \leq 4$ , there is only one second-order phase transition from the long-range ordered phase to the disordered phase. The

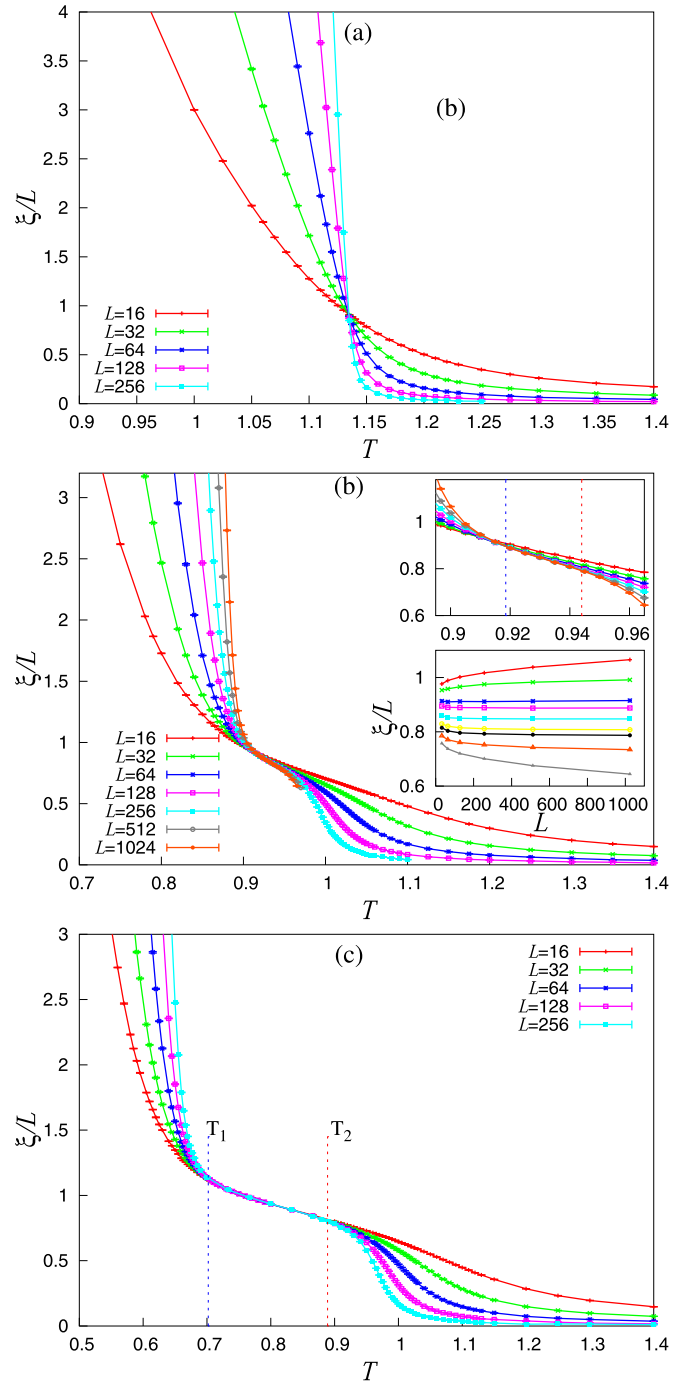


FIG. 5. The temperature dependence of the correlation length ratio for three cases:  $q = 4$  (a),  $q = 5$  (b), and  $q = 6$  (c). The upper inset of (b) presents the merging segment of  $\xi/L$  between  $T_1$  and  $T_2$  for  $q = 5$ . The lower inset of (b) describes  $\xi/L$  versus  $L$  for  $q = 5$  at several temperatures  $T = 0.90, 0.905, 0.915, 0.920, 0.930, 0.940, 0.945, 0.955, 0.965$  from top to bottom.

critical temperature  $T_c$  is easily defined at the crossing point of Binder ratio curves as in the  $q = 4$  case. For  $q \geq 5$ , both phase transitions are KT type, at  $T_2$  from the quasi-long-range ordered phase to the disordered phase, and at  $T_1$  from the long-range ordered phase to the quasi-long-range ordered phase.

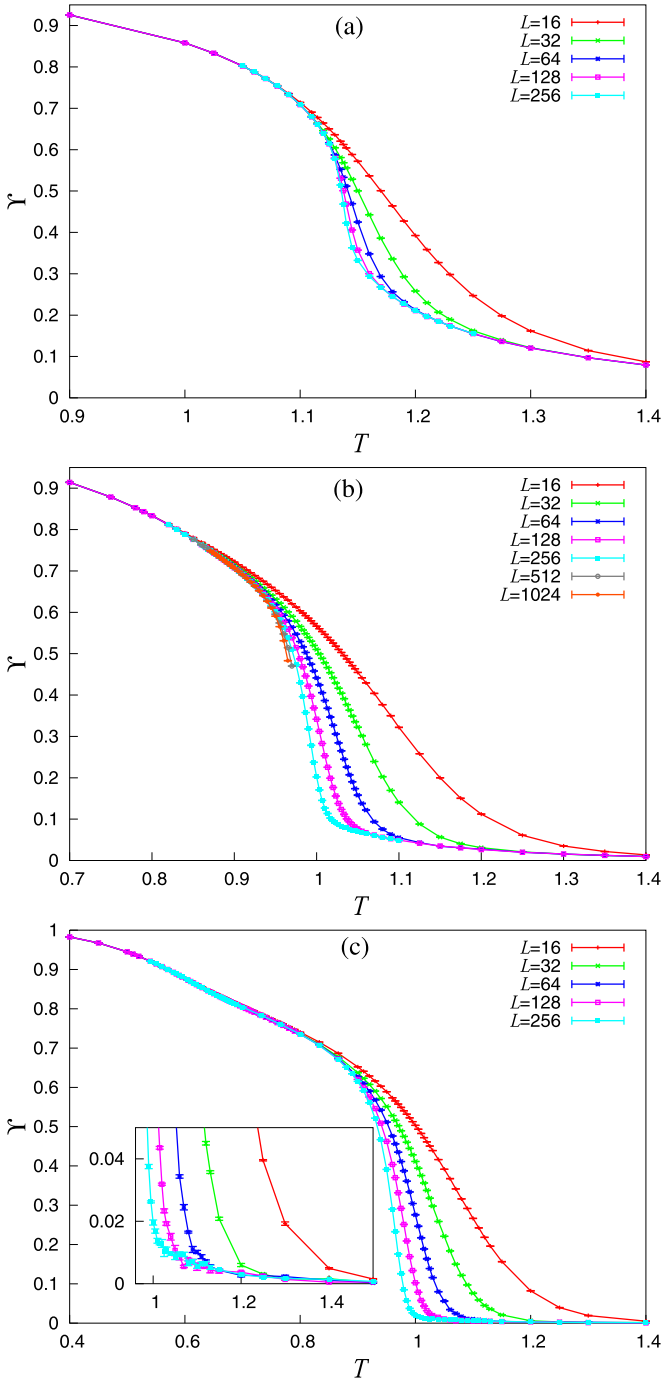


FIG. 6. The helicity modulus versus temperature for  $q = 4$  (a),  $q = 5$  (b), and  $q = 6$  (c). Enlarged plot in (c) presents the nonvanishing of  $\Upsilon$  for  $q = 6$  in the high-temperature region.

These critical temperatures  $T_1$  and  $T_2$  are determined from the negative divergent dips of the derivative of the Binder ratio as in cases of  $q = 5, 6$ .  $T_2(q)$  is nearly flat, roughly the critical temperature of the KT transition of the 2D XY model (i.e., the limit  $q \rightarrow \infty$ ), while  $T_1(q)$  monotonically decreases to 0 as  $q$  increases. Our critical temperatures,  $T_1$  and  $T_2$ , agree with previous works obtained by different approaches [15,31].

Next, we consider the behavior of the correlation length ratio around the critical points. Figure 5 illustrates the corre-

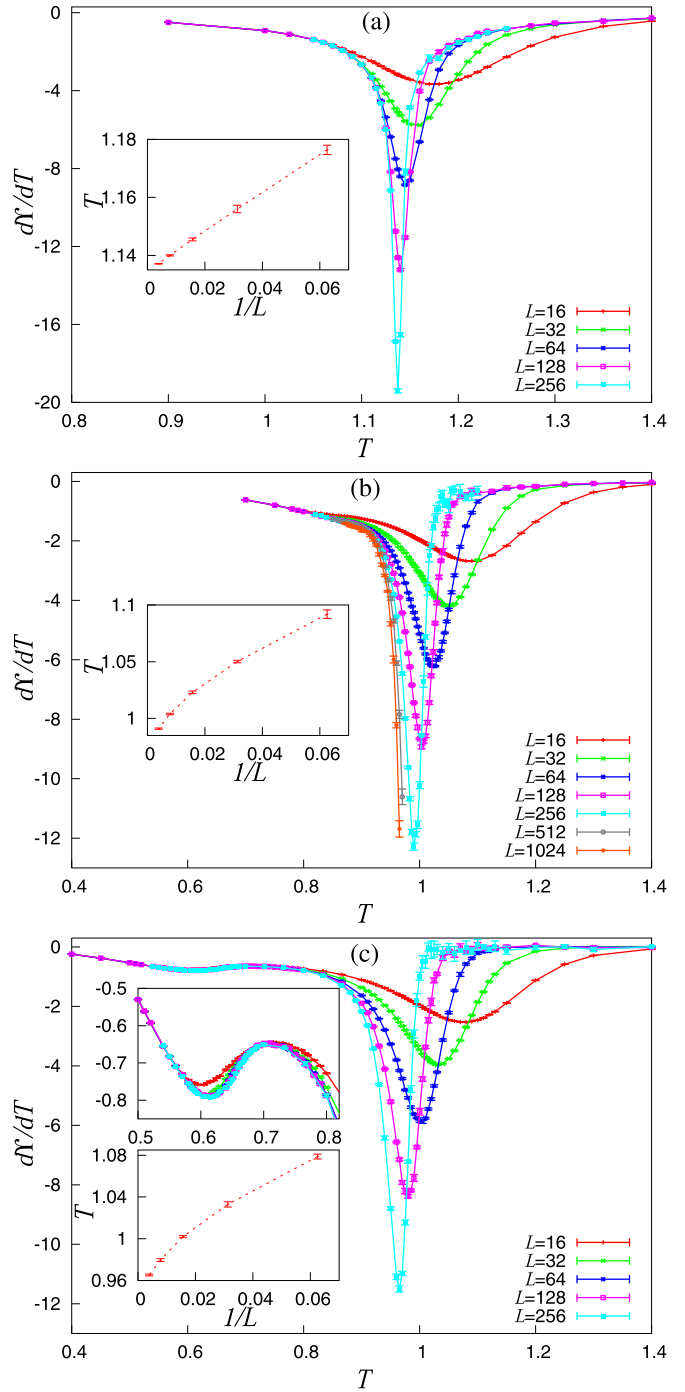


FIG. 7. The temperature derivative of the helicity modulus versus temperature for  $q = 4$  (a),  $q = 5$  (b), and  $q = 6$  (c). The dip temperatures  $T_c^{\Upsilon}(L)$  for  $q = 4$  and  $T_2^{\Upsilon}(L)$  for  $q = 5, 6$  versus  $1/L$  are shown in the inset of (a), the inset of (b), and the lower inset of (c), respectively. The enlarged plot in the upper inset of (c) presents a tiny dip below  $T_1$  for  $q = 6$ .

lation length ratio as a function of temperature for  $q = 4, 5, 6$ . This result of  $\xi/L$  for  $q = 5$  and  $6$  is consistent with the previous work of Surungan *et al.* [9]. For  $q = 4$ , in Fig. 5(a),  $\xi/L$  curves with different  $L$  cross at the critical temperature  $T_c \approx 1.135$ , the same as our estimation by the Binder ratio. For  $q = 5$  and  $6$ , in Figs. 5(b) and 5(c),  $\xi/L$  decreases towards zero in

the high-temperature region (disordered phase) and increases to infinity in the low-temperature region (ordered phase). Moreover, in the intermediate-temperature region  $T_1 < T < T_2$ ,  $\xi/L$  tends to be independent of  $L$ , which is indeed a characteristic of the quasi-long-range ordered phase. This is rather clear for  $q = 6$ : the critical temperatures for  $q = 6$  estimated approximately from Fig. 5(c) are  $T_1 \approx 0.7$  and  $T_2 \approx 0.89$ . The independence of  $L$  for  $q = 5$  is not very clear as in  $q = 6$  case, even by magnifying  $\xi/L$  in  $[T_1, T_2]$  [see the upper inset of Fig. 5(b)]. Therefore, we show  $\xi/L$  versus  $L$  for several temperatures between 0.90 and 0.965 in the lower inset of Fig. 5(b). As  $L$  increases,  $\xi/L$  increases for low temperatures  $T = 0.90, 0.905$  (characteristic of an ordered phase), decreases for high temperatures  $T = 0.955, 0.965$  (characteristic of a disordered phase), and is almost constant for several intermediate temperatures  $T = 0.920, 0.930, 0.940$ . This suggests that  $\xi/L$  becomes independent of  $L$  in the intermediate temperature range  $[0.920, 0.940]$ , that is a characteristic of the quasi-long-range ordered phase.

Next, we show the helicity modulus,  $\Upsilon$ , as a function of temperature for  $q = 4, q = 5$ , and  $q = 6$  in Fig. 6. For  $q = 4$  and  $q = 5$ ,  $\Upsilon$  does not vanish in the high-temperature disordered phase. These results are consistent with numerical results of Kumano *et al.* ( $q = 5$ ) [8] and Baek *et al.* ( $q = 4$  and  $q = 5$ ) [6]. For  $q = 6$ , we find out that  $\Upsilon$  also does not vanish in the high-temperature disordered phase [see the inset of Fig. 6(c)]. This observation of  $\Upsilon$  for  $q = 6$  disagrees with previous numerical works [6,8], but agrees with the analytical work of Kumano *et al.* [8]. Therefore, the conclusion about non-KT phase transition based on the nonvanishing of  $\Upsilon$  in the high-temperature region by Baek *et al.* [6] is invalid for the 2D  $q$ -state clock model.

Finally, the data of  $d\Upsilon/dT$  for  $q = 4, q = 5$ , and  $q = 6$  as a function of temperature are shown in Fig. 7. These results are similar to previous work in the high-temperature region [6]. For  $q = 4$ ,  $d\Upsilon/dT$  has a negative divergent dip at nearly  $T_c$ . As  $L \rightarrow \infty$ , the dip temperature  $T_c^\Upsilon(L)$  monotonically shifts toward  $T_c$  as a linear form  $\sim 1/L$  [see the inset of Fig. 7(a)]. This behavior reconfirms that the phase transition of the case  $q = 4$  is second order. For  $q = 5$  and  $q = 6$ , there also appears a negative divergent dip of  $d\Upsilon/dT$  around  $T_2$

but the dip temperature  $T_2^\Upsilon(L)$  gradually shifts toward the critical temperature  $T_2$  as a nonlinear form of  $1/L$  [see insets of Figs. 7(b) and 7(c)]. This size-dependent behavior of  $T_2^\Upsilon(L)$  from  $d\Upsilon/dT$  suggests that phase transitions at  $T_2$  for  $q = 5, 6$  are not second order. On the other hand, the helicity modulus and its derivative do not show any clear signal of the phase transition at  $T_1$  for  $q = 5, 6$  [see the upper inset of Fig. 7(c)].

#### IV. CONCLUSIONS

In this paper, we study the phase transition phenomena of the 2D  $q$ -state clock model for  $q = 4, q = 5$ , and  $q = 6$  by Monte Carlo simulation. Several physical quantities including the Binder ratio, the derivative of the Binder ratio, the correlation length ratio, the helicity modulus, and the derivative of the helicity modulus are calculated for this model. Our numerical results show that the helicity modulus is not a suitable quantity to detect the KT phase transition both for  $q = 5$  and for  $q = 6$ . On the other hand, the Binder ratio and the correlation length ratio can show the existence of two distinct KT phase transitions for  $q = 5$ .

We show that the conventional Binder ratio is capable of detecting the KT phase transition between the quasi-long-range ordered phase and the long-range ordered phase in the 2D  $q$ -state clock model. We also reconstruct the phase diagram of the 2D  $q$ -state clock model by analyzing a unique physical quantity, the conventional Binder ratio. Although our technique using the Binder ratio to determine critical points in this paper is only for a simple model, the  $q$ -state clock model, it can be readily applied to generalized discrete spin models or generalized XY spin models.

#### ACKNOWLEDGMENTS

This research is funded by Vietnam National Foundation for Science and Technology Development (NAFOSTED) under Grant No. 103.05-2019.44. Numerical calculation was performed using computers at the Advanced Institute for Science and Technology, Hanoi University of Science and Technology.

- 
- [1] J. V. Jose, L. P. Kadanoff, S. Kirkpatrick, and D. R. Nelson, Renormalization, vortices, and symmetry-breaking perturbations in the two-dimensional planar model, *Phys. Rev. B* **16**, 1217 (1977).
  - [2] S. Elitzur, R. B. Pearson, and J. Shigemitsu, Phase structure of discrete Abelian spin and gauge systems, *Phys. Rev. D* **19**, 3698 (1979).
  - [3] J. Tobochnik, Properties of the  $q$ -state clock model for  $q = 4, 5$ , and 6, *Phys. Rev. B* **26**, 6201 (1982).
  - [4] Murty S. S. Challa and D. P. Landau, Critical behavior of the six-state clock model in two dimensions, *Phys. Rev. B* **33**, 437 (1986).
  - [5] H. Matsuo and K. Nomura, Berezinskii-Kosterlitz-Thouless transitions in the six-state clock model, *J. Phys. A: Math. Gen.* **39**, 2953 (2006).
  - [6] S. K. Baek and P. Minnhagen, Non-Kosterlitz-Thouless transitions for the  $q$ -state clock models, *Phys. Rev. E* **82**, 031102 (2010).
  - [7] G. Ortiz, E. Cobanera, and Z. Nussinov, Dualities and the phase diagram of the p-clock model, *Nucl. Phys. B* **854**, 780 (2012).
  - [8] Y. Kumano, K. Hukushima, Y. Tomita, and M. Oshikawa, Response to a twist in systems with  $Z_p$  symmetry: The two-dimensional  $p$ -state clock model, *Phys. Rev. B* **88**, 104427 (2013).
  - [9] T. Surungan, S. Masuda, Y. Komura, and Y. Okabe, Berezinskii-Kosterlitz-Thouless transition on regular and Villain types of  $q$ -state clock models, *J. Phys. A: Math. Theor.* **52**, 275002 (2019).
  - [10] N. D. Mermin and H. Wagner, Absence of Ferromagnetism or Antiferromagnetism in One- or Two-Dimensional Isotropic Heisenberg Models, *Phys. Rev. Lett.* **17**, 1307 (1966).

- [11] J. M. Kosterlitz and D. J. Thouless, Ordering, metastability and phase transitions in two-dimensional systems, *J. Phys. C* **6**, 1181 (1973).
- [12] V. I. Marconi and D. Dominguez, Nonequilibrium Transitions in Fully Frustrated Josephson Junction Arrays, *Phys. Rev. Lett.* **87**, 017004 (2001).
- [13] Richard L. C. Vink, Crossover from a Kosterlitz-Thouless phase transition to a discontinuous phase transition in two-dimensional liquid crystals, *Phys. Rev. E* **90**, 062132 (2014).
- [14] D. Podolsky, E. Shimshoni, G. Morigi, and S. Fishman, Buckling Transitions and Clock Order of Two-Dimensional Coulomb Crystals, *Phys. Rev. X* **6**, 031025 (2016).
- [15] C. M. Lapilli, P. Pfeifer, and C. Wexler, Universality Away from Critical Points in Two-Dimensional Phase Transitions, *Phys. Rev. Lett.* **96**, 140603 (2006).
- [16] C. Chatelain, DMRG study of the Berezinskii-Kosterlitz-Thouless transitions of the 2D five-state clock model, *J. Stat. Mech.* (2014) P11022.
- [17] D. X. Viet and H. Kawamura, Monte Carlo studies of chiral and spin ordering of the three-dimensional Heisenberg spin glass, *Phys. Rev. B* **80**, 064418 (2009).
- [18] Y. Komura and Y. Okabe, Large-scale monte carlo simulation of two-dimensional classical XY model using multiple GPUs, *J. Phys. Soc. Jpn.* **81**, 113001 (2012).
- [19] C. Ding, W. Guo, and Y. Deng, Reentrance of Berezinskii-Kosterlitz-Thouless-like transitions in a three-state Potts anti-ferromagnetic thin film, *Phys. Rev. B* **90**, 134420 (2014).
- [20] H. G. Ballesteros, A. Cruz, L. A. Fernandez, V. Martin-Mayor, J. Pech, J. J. Ruiz-Lorenzo, A. Tarancon, P. Tellez, C. L. Ullod, and C. Ungil, Critical behavior of the three-dimensional Ising spin glass, *Phys. Rev. B* **62**, 14237 (2000).
- [21] M. Hasenbusch, The Binder cumulant at the Kosterlitz-Thouless transition, *J. Stat. Mech.* (2008) P08003.
- [22] D. X. Nui, L. Tuan, N. D. Trung Kien, P. T. Huy, H. T. Dang, and D. X. Viet, Correlation length in a generalized two-dimensional XY model, *Phys. Rev. B* **98**, 144421 (2018).
- [23] D. Loison, Binder's cumulant for the Kosterlitz-Thouless transition, *J. Phys.: Condens. Matter* **11**, L401 (1999).
- [24] O. Borisenko, G. Cortese, R. Fiore, M. Gravina, and A. Papa, Numerical study of the phase transitions in the two-dimensional Z(5) vector model, *Phys. Rev. E* **83**, 041120 (2011).
- [25] K. Binder, Finite size scaling analysis of Ising model block distribution functions, *Z. Phys. B* **43**, 119 (1981).
- [26] E. Rastelli, S. Regina, and A. Tassi, Monte Carlo simulation of a planar rotator model with symmetry-breaking fields, *Phys. Rev. B* **69**, 174407 (2004).
- [27] M. Nishino and S. Miyashita, Termination of the Berezinskii-Kosterlitz-Thouless phase with a new critical universality in spin-crossover systems, *Phys. Rev. B* **92**, 184404 (2015).
- [28] F. Alet, Y. Ikhlef, J. L. Jacobsen, G. Misguich, and V. Pasquier, Classical dimers with aligning interactions on the square lattice, *Phys. Rev. E* **74**, 041124 (2006).
- [29] S. K. Baek, P. Minnhagen, and B. J. Kim, True and quasi-long-range order in the generalized  $q$ -state clock model, *Phys. Rev. E* **80**, 060101(R) (2009).
- [30] Y. Tomita and Y. Okabe, Probability-changing cluster algorithm for two-dimensional XY and clock models, *Phys. Rev. B* **65**, 184405 (2002).
- [31] S. Chatterjee, S. Puri, and R. Paul, Ordering kinetics in the  $q$ -state clock model: Scaling properties and growth laws, *Phys. Rev. E* **98**, 032109 (2018).